Available online at www.sciencedirect.com
ScienceDirect
Polymer 47 (2006) 7034–7042
polymer
www.elsevier.com/locate/polymer

The anomalous melting behavior of water in aqueous PVME solutions

Els Loozen [a], Kurt Van Durme [b], Erik Nies [a,c,*], Bruno Van Mele [b,**], Hugo Berghmans [a]

[a] *Polymer Research Division, Department of Chemistry, Katholieke Universiteit Leuven, 3001 Heverlee, Belgium*
[b] *Faculty of Engineering, Department of Physical Chemistry and Polymer Science – FYSC, Vrije Universiteit Brussel – VUB, Pleinlaan 2, B-1050 Brussels, Belgium*
[c] *Laboratory of Polymer Technology, Eindhoven University of Technology, The Netherlands*

Received 25 April 2006; received in revised form 31 July 2006; accepted 3 August 2006
Available online 28 August 2006

Abstract

The Wertheim lattice thermodynamic perturbation theory is used to predict the liquid–liquid and solid–liquid coexistence data for a model polymer solution. The theory predicts bimodal LCST phase behavior and an unusual step with composition in the solid–liquid equilibrium of the solvent.

The theoretical solid–liquid equilibrium calculations are used to interpret experimental data obtained for aqueous solutions of poly(vinyl methyl ether) (PVME), which is known to show bimodal LCST phase behavior. An experimental method is proposed, employing Fourier transform infrared (FTIR) spectroscopy to determine the equilibrium melting line of water in the presence of PVME. In addition, the complete melting line of water is obtained by partial integration of the melting endotherm observed using modulated temperature differential scanning calorimetry (MTDSC). Both, the FTIR and MTDSC methods are in good agreement, experimentally confirming the predicted step with composition in the solid–liquid equilibrium. This peculiar concentration dependence of the melting curve of ice provides a new explanation for the inhibited crystallization of water in aqueous PVME solutions, since the actual supercooling (at high polymer concentration) is smaller than it could be anticipated for a conventional course of the melting curve. Hence, the vicinity of the glass transition region in these highly concentrated polymer mixtures leads to a dramatic slowing down of the nucleation rate and thus the subsequent crystallization. Moreover, the atypical shape of the equilibrium melting line also provides a new explanation for the double melting endotherm observed in (MT)DSC experiments, which is conventionally attributed to the melting at different temperatures of bound and free water.

Keywords: Poly(vinyl methyl ether); Water; Anomalous melting behavior

1. Introduction

The binary mixture poly(vinyl methyl ether) (PVME)/water shows a bimodal lower critical solution temperature (LCST) liquid–liquid miscibility gap at ca. 35 °C [1,2]. Moreover, in highly concentrated mixtures with mass fraction of PVME, $w_{PVME} > 0.6$ the crystallization of water cannot be achieved by simply lowering the temperature at typical cooling rates used in e.g. DSC experiments [3]. A similar low-temperature behavior has been observed for aqueous solutions of poly(*N*-isopropyl acrylamide) (PNIPAM) [4,5] and poly(*N*-vinyl caprolactam) (PVCL) [6], in which the lack of crystallization of water at high polymer concentration is ascribed to the interference of vitrification of the homogeneous solution with the crystallization process. On the other hand, because of the low glass transition temperature of PVME ($T_g \sim -25$ °C) the absence of crystallization of water in the aqueous PVME system was not attributed to vitrification, but was interpreted to give evidence to the existence of a stable polymer/solvent complex in which two water molecules are hydrogen bonded to the PVME repeating unit [7,8].

However, further investigation demonstrated that for $w_{PVME} \approx 0.7$ the crystallization of water could be realized once ice nuclei are added [3]. This experiment casts doubt

* Corresponding author. Laboratory of Polymer Technology, Eindhoven University of Technology, P.O. Box 513, 5600MB Eindhoven, The Netherlands. Tel.: +31 40 2474954; fax: +31 40 2436999.
** Corresponding author. Tel.: +32 2 6293288; fax: +32 2 6293278.
E-mail addresses: e.l.f.nies@tue.nl (E. Nies), bvmele@vub.ac.be (B. Van Mele).

0032-3861/$ - see front matter © 2006 Elsevier Ltd. All rights reserved.
doi:10.1016/j.polymer.2006.08.003

on the existence of stable molecular complexes and indicates that the inhibited crystallization of water, in highly concentrated mixtures, is related to crystal nucleation problems, rather than being linked to the existence of a stable intermolecular complex. Still, for a conventional course of the melting line this is quite unexpected as a sufficient supercooling in such mixture should be feasible, by which nucleation and subsequent crystallization are triggered before the vicinity of the glass transition region slows down these processes.

In addition to these experimental observations, theoretical calculations for a model polymer solution involving saturation interactions (which are an appropriate model for hydrogen-bonding interactions) between solvent molecules and either polymer segments or other solvent molecules were performed, using the thermodynamic perturbation theory of Wertheim [9,10] adapted to the lattice model [11]. In this way molecular understanding of such peculiar phase behavior could be obtained. The Wertheim lattice thermodynamic perturbation theory (Wertheim-LTPT) predicts bimodal LCST miscibility in agreement with experimental observation [12], which is the first time that a theory predicts the occurrence of bimodal phase behavior. Thus far this could only be phenomenologically described using an extended composition and temperature dependent Flory–Huggins interaction function [13]. In addition to the bimodal phase behavior, and closely connected to it, two adjacent upper critical solution temperature (UCST) miscibility gaps at low temperature are predicted [12]. Furthermore, the calculated melting line of the solvent displays an unusual step with composition, which becomes more pronounced when the equilibrium melting temperature is located at lower temperatures. In order to verify this prediction, it is of interest to experimentally determine the melting line of water in aqueous PVME solutions and to establish whether this experimental melting line contains the predicted peculiar shape or, conversely, indeed abruptly stops near $w_{PVME} > 0.6$, pointing to the existence of a polymer/solvent complex.

In this work we will solely focus on the crystallization/melting behavior of the solvent. In this respect Fourier transform infrared (FTIR) spectroscopy is employed to determine the equilibrium melting line of water starting from a mixture composition for which the crystallization of water can be achieved upon cooling. In this way the composition of the polymer/water mixture in coexistence with ice is determined in situ at any temperature of the solid–liquid equilibrium, by which the equilibrium melting line within the entire concentration range can be obtained. The FTIR results are compared to the melting temperatures of water in the presence of PVME determined directly from non-isothermal modulated temperature DSC (MTDSC) experiments or by partial integration of the MTDSC melting endotherm observed.

2. Materials and experimental methods

2.1. Materials

Poly(vinyl methyl ether) (PVME) was purchased from Aldrich as an aqueous solution (mass fraction PVME, $w_{PVME} = 0.5$). In order to obtain the pure polymer the mixture was diluted with de-ionized water to $w_{PVME} = 0.1$. This solution was heated to ca. 50 °C to induce liquid–liquid phase separation. The concentrated phase was isolated and dried at 60 °C under vacuum for several days. The PVME mass average molar mass, M_w, equals 20 kg mol^{-1}, determined by small angle neutron scattering (SANS) [13].

2.2. Sample preparation

2.2.1. FTIR experiments

A range of homogeneous PVME/water mixtures were prepared by adding appropriate amounts of water to dried PVME. These samples were allowed to homogenize at room temperature in closed recipients for periods up to two months for the highest polymer concentrations. The mixtures were regularly mechanically mixed. Mixture compositions are expressed in mass fraction PVME in the PVME/H_2O mixture, w_{PVME}.

2.2.2. MTDSC experiments

A range of compositions were prepared by adding the appropriate amount of water to dried PVME directly in Mettler aluminum pans that were subsequently hermetically sealed. The inserted sample mass typically varied between 0.5 and 5 mg. These samples were stored at 4 °C for at least one month to become homogeneous. A few of the closed crucibles were perforated and the water evaporation was measured at 100 °C to check the preparation procedure using thermogravimetric analysis (TGA) (error on polymer mass fraction is <0.001).

2.3. Experimental methods

2.3.1. Fourier transform infrared (FTIR) spectroscopy

A Perkin Elmer FTIR 2000 spectrometer was used. The sample solutions were put between two calcium fluoride (CaF_2) windows (without a spacer), pressed together to get IR absorbance readings below 1 (to assure non-saturated IR signals) and placed in a temperature controlled cell (SPECAC), connected to a Julabo thermostat bath. A thermocouple attached to the temperature cell was used to attain accurate temperature readings. Background spectrum was obtained using a blank CaF_2 window. Ten interferograms, taken with a spectral resolution of 2 cm^{-1}, were superimposed to obtain a good signal-to-noise ratio. The standard deviations in temperature and reading of the FTIR wavenumbers are estimated to be 0.5 °C and 1 cm^{-1}, respectively.

2.3.2. Modulated temperature differential scanning calorimetry (MTDSC)

A first series of MTDSC measurements were performed on a TA Instruments 2920 DSC with the MDSC™ option and a refrigerated cooling system. Helium was used as a purge gas (25 mL min^{-1}). Indium and cyclohexane were used for temperature calibration. The former was also used for enthalpy calibration. A second series of MTDSC experiments were performed on a TA Instruments Q1000 (T-zero™ DSC-technology) with

a liquid nitrogen cooling system. Nitrogen was used as a purge gas (25 mL min^{-1}). *n*-Decane and cyclohexane were used for temperature calibration. The former was also used for enthalpy calibration.

Standard modulation conditions, in both experimental series, are an amplitude of 0.50 °C with a period of 60 s. Heat capacity calibration was performed in standard modulation conditions with water, using the heat capacity difference between two temperatures, one above and one below the melting temperature. In this way, the most accurate measurements of heat capacity changes and excess contributions, c_p^{excess}, were obtained. Data are expressed as specific heat capacities (or changes) in J g^{-1} K^{-1}. Non-isothermal experiments were performed at an underlying heating/cooling rate of 1 °C min^{-1}.

3. Theoretical section

3.1. The Wertheim lattice thermodynamic perturbation theory

From the theoretical point of view it is of interest to investigate the complicated phase behavior of systems involving hydrogen-bonding interactions using a theoretical approach that incorporates directly and explicitly the formation of specific interactions. The seminal work of Wertheim concerning saturation interactions is applied, whereby the Wertheim theory is mapped onto the lattice model that is also the basis for the Flory–Huggins theory [9–11,14]. Here we summarize the essential equations needed to describe the phase behavior. Details about the Wertheim-LTPT can be found elsewhere [11].

The lattice positions, N_L in total, have co-ordination number z and are occupied either by a solvent molecule (component 0) or by a segment of a polymer molecule (component 1). Each molecule of component 0 carries a specific site A and each segment of component 1 carries a specific site B. Nearest neighbor molecules and segments interact by dispersive interactions with an interaction energy, $-\varepsilon_{ij}(i,j=0,1)$, depending on the pair of units (solvent molecules or polymer segments) involved. Furthermore, the specific sites A on molecules of type 1 interact with interaction strength $-\varepsilon_{00}^{AA}$ if they are properly oriented relative to each other and specific sites A and B interact with interaction strength $-\varepsilon_{01}^{AB} = -\varepsilon_{10}^{BA}$. No specific interactions exist between sites B, i.e., $\varepsilon_{11}^{BB} = 0$.

In the thermodynamic perturbation theory of Wertheim the excess Gibbs free energy per lattice site can be written as a sum, according to the following equation:

$$\Delta G/N_L kT = \Delta G_R/N_L kT + \Delta G_{NN}/N_L kT + \Delta G_{AB}/N_L kT \qquad (1)$$

with k being the Boltzmann constant and T the absolute temperature.

The excess Gibbs free energy of the reference system, ΔG_R, is the excess free enthalpy of the same system excluding both nearest neighbor and specific interactions. In the Wertheim-LTPT the Flory–Huggins (FH) combinatorial entropy is recovered:

$$\frac{\Delta G_R}{N_L kT} = \phi_0 \ln \phi_0 + \frac{\phi_1}{s_1} \ln \phi_1 \qquad (2)$$

with s_1 being the number of segments in a polymer chain, and ϕ_i the segment fraction of component i.

For the free energy of nearest neighbor interactions the following mean field approximation is used:

$$\frac{\Delta G_{NN}}{N_L kT} = \frac{z\Delta w}{2kT}\ \phi_0\phi_1 = \chi\phi_0\phi_1 \qquad (3)$$

with χ being the Flory–Huggins interaction parameter and $\Delta w = 2(-\varepsilon_{01}) - ((-\varepsilon_{00}) + (-\varepsilon_{11}))$, the exchange energy defined for the nearest neighbor dispersive interactions, which is in the FH theory the only relevant energy scale. The FH exchange energy can also serve to define a reduced temperature $T^* = 2kT/z\Delta w$, which will be used in the calculations and the representation of the predictions.

The sum of Eqs. (2) and (3) constitutes the standard Flory–Huggins mixture (or solution) theory in its most simple mean field approximation. Although the FH theory does not provide a quantitative prediction of the actual phase behavior of the model system, it does capture its essence. Moreover, we do not wish to introduce additional empirical parameters making the theory semi-empirical at most. Therefore, the theory will not be used to fit the experimental data as this would only provide empirical parameters that describe within the limitations of the simple theory the experimental system in the most optimal but empirical way. Alternatively, the theory is applied to predict the overall phase behavior (both above and below 0 °C), which also leads to non-trivial predictions of the melting line of the solvent when saturation interactions are involved. These predictions are derived from theoretical parameter values that were established in earlier work with the intention of describing bimodal LCST phase behavior [13]. The remaining parameters required to describe the solid–liquid equilibrium are varied within certain limits (see Section 4).

The excess free enthalpy due to the association between A sites and A and B sites, respectively, is given by the following equation:

$$\frac{\Delta G_{AB}}{N_L kT} = \phi_0\left[\ln X_A^0 - \frac{X_A^0}{2} + \frac{1}{2}\right] + \phi_1\left[\ln X_B^1 - \frac{X_B^1}{2} + \frac{1}{2}\right] \qquad (4)$$

with $X_A^0 (X_B^1)$ being the fraction of non-bonded sites A (B).

These fractions are determined from the set of equations:

$$\overline{X}_A(1 + \overline{X}_A\Delta_{AA} + \overline{X}_B\Delta_{AB}) - \phi_0 = 0$$

$$\overline{X}_B(1 + \overline{X}_A\Delta_{AB} + \overline{X}_B\Delta_{BB}) - \phi_1 = 0 \qquad (5)$$

where $\overline{X}_A = \phi_0 X_A^0$, $\overline{X}_B = \phi_1 X_B^1$.

The parameter $\Delta_{\alpha\beta}(\alpha,\beta = \text{A or B})$ in Eq. (5) is given by

$$\Delta_{\alpha\beta} = K\left(\exp\left(\varepsilon_{ij}^{\alpha\beta}/kT\right) - 1\right) \qquad (6)$$

with K being the ratio of the nearest neighbor positions with the proper orientation to all possible orientations.

3.1.1. Liquid–liquid equilibrium calculations

Thermodynamic properties are easily calculated, using the excess Gibbs free energy, given by Eq. (1). In particular, spinodal and critical conditions can be derived by considering the second and third compositional derivatives of the Gibbs free energy:

$$J_{sp} = \left.\frac{\partial^2 \Delta G/N_L kT}{\partial \phi_1^2}\right|_{T,p} = 0 \text{ and } J_{cr} = \left.\frac{\partial^3 \Delta G/N_L kT}{\partial \phi_1^3}\right|_{T,p} = 0 \qquad (7)$$

The critical temperature and composition are given by the simultaneous set of Eq. (7), while at the spinodal only $J_{sp} = 0$ is obeyed.

The liquid–liquid coexistence curves are calculated using the standard equilibrium conditions:

$$\Delta\mu_0' = \Delta\mu_0'' \text{ and } \Delta\mu_1' = \Delta\mu_1'' \qquad (8)$$

with $\Delta\mu_0^{\prime(\prime\prime)}$ and $\Delta\mu_1^{\prime(\prime\prime)}$ being the excess chemical potential of the solvent (0) and polymer (1) in the coexisting liquid mixture phases, denoted by single and double primes. The excess chemical potential of component i, $\Delta\mu_i$, in the polymer solution can be calculated from the excess Gibbs free energy, according to the standard thermodynamic definition:

$$\Delta\mu_i = \left.\frac{\partial \Delta G}{\partial N_i}\right|_{T,p,N_j \neq N_i}$$

3.1.2. Solid–liquid equilibrium calculations

The melting temperature of the crystalline solvent in equilibrium with a liquid polymer/solvent mixture can be calculated from the equilibrium condition:

$$\Delta\mu_0 = \Delta\mu_{0,\text{solid}}^0 \qquad (9)$$

with $\Delta\mu_0(\Delta\mu_{0,\text{solid}}^0)$ being the excess chemical potential of the solvent in the liquid mixture (pure solid crystalline) phase. In order to obtain the excess chemical potential $\Delta\mu_{0,\text{solid}}^0$ of the pure crystalline solvent at the temperature $T_{m,0}$ the standard thermodynamic model is adapted:

$$\frac{\Delta\mu_{0,\text{solid}}^0}{kT_{m,0}} = \frac{\Delta H_{m,0}^0}{k}\left(\frac{1}{T_{m,0}^0} - \frac{1}{T_{m,0}}\right) = \frac{\Delta H_{m,0}^0}{z\Delta w/2}\left(\frac{z\Delta w/2}{kT_{m,0}^0} - \frac{z\Delta w/2}{kT_{m,0}}\right)$$
$$= \Delta H_{m,0}^{0\,*}\left(\frac{1}{T_{m,0}^{0\,*}} - \frac{1}{T_{m,0}^*}\right) \qquad (10)$$

with $\Delta H_{m,0}^0$ and $T_{m,0}^0$ being the enthalpy of fusion and the equilibrium melting temperature of the pure component 0, respectively. The third equality in Eq. (10) defines the reduced enthalpy of fusion and the reduced melting temperatures.

Eqs. (1)–(10) will be used to calculate the liquid–liquid miscibility behavior and the solid–liquid coexistence line.

4. Results and discussion

4.1. Theory: the Wertheim lattice thermodynamic perturbation theory, theoretical phase behavior for a model polymer solution

In Fig. 1 the predicted bimodal LCST binodal, spinodal and critical conditions are shown for a model polymer solution. The parameters used for these predictions are taken from previous work [13] and are tabulated in Table 1. It is the first time that a theory predicts bimodal LCST phase behavior. So far bimodality was only phenomenologically described with an extended composition and temperature dependent Flory–Huggins interaction function. The occurrence of the bimodal LCST miscibility gap strongly depends on the interaction strength of the saturation interactions between both components. That is, bimodality is only observed when the solvent–polymer interaction is (somewhat) stronger than the solvent–solvent interaction (calculations not shown). This has been discussed previously [13].

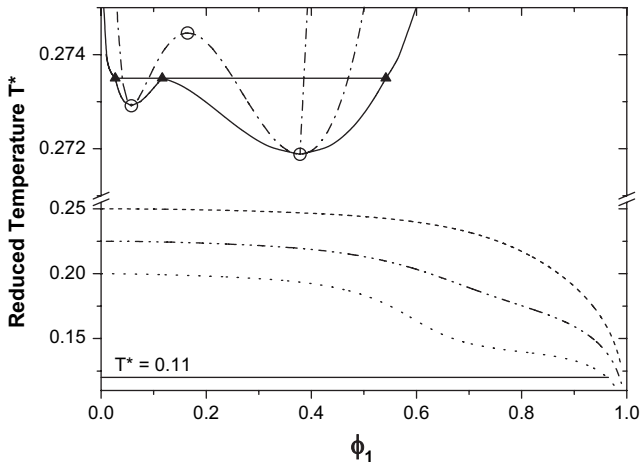

Fig. 1. Theoretical reduced temperature-composition ($T^* - \phi_1$) phase diagram of a model polymer solution. Predicted LCST spinodal (—·—·—), binodal (——) and critical conditions (o). Predicted melting temperature $T_{m,0}^*$ of the solvent versus composition for three values of $T_{m,0}^{0\,*}$: 0.250 (- - - - -), 0.225 (·····) and 0.200 (·····). The horizontal solid line at $T^* = 0.11$ represents the tie line connecting the two phases in equilibrium governed by the solid–liquid equilibrium (solid ice, $\phi_1 = 0$, and a highly concentrated polymer solution, $\phi_1 = 0.965$). Parameter values used in the calculations are summarized in Table 1.

Table 1
Parameter values in the Wertheim-LTPT used to calculate the phase behavior depicted in Fig. 1

Parameter	Value	Parameter	Value
s_1	100	K_{00}^{AA}	6
z	6	$K_{01}^{AB} = K_{10}^{BA}$	495
ε_{01}/k	−0.1	$\Delta H_{m,0}^{0\,*}$	1.500
$\varepsilon_{00}/k = \varepsilon_{11}/k$	0	$T_{m,0}^{0\,*}$	0.200, 0.225, 0.250
ε_{00}^{AA}/k	1.5		
$\varepsilon_{01}^{AB}/k = \varepsilon_{10}^{BA}/k$	2.8		

These values are taken from previous work [13].

The solid–liquid equilibrium of the solvent is determined by considering the standard thermodynamic relationships for the solvent crystalline phase (Eq. (10)). The calculated solvent melting line is also shown in Fig. 1 for different values of the (reduced) equilibrium melting temperature of the solvent $T^{0}_{m,0}{}^{*}$. It displays an unusual step with composition, which becomes more pronounced as $T^{0}_{m,0}{}^{*}$ is located at lower temperatures.

4.2. Experimental results

4.2.1. Literature indication of the peculiar solid–liquid equilibrium line

There already exist experimental indications for the predicted peculiar shape of the melting line of the solvent when analyzing more carefully previously presented dilatometric and calorimetric results on PVME/water (see Fig. 2 and in Ref. [3]: Figs. 3, 4 and 6). These experimental data reveal, in principle, the course of the melting line, since both the variation of the dilatometric volume and the shape of the DSC melting endotherm are a direct consequence of the concentration–temperature dependence of the melting line of ice, being determined by the thermodynamic solid–liquid equilibrium conditions.

The observed volume change with temperature from Fig. 2, in the temperature interval where ice and a liquid polymer solution coexist, is dominated by the volume change accompanying the melting of ice. The additional volume change due to the mixing of liquid water with the surrounding polymer solution is much smaller and can be ignored in first approximation. Hence, the shape of the dilatometric trace reflects the evolution of the melting line. Note that the dilatometric measurement actually yields equilibrium conditions if, at each temperature, the system is given sufficient time to reach the equilibrium state.

To illustrate this reasoning we assume that the shape of the melting line is given by the dotted line in Fig. 1. At very low (reduced) temperatures ($T^{*} = 0.11$; Fig. 1, solid line) ice is in equilibrium with a highly concentrated polymer mixture ($\phi_1 = 0.965$) of which the composition slightly changes upon raising the temperature, until the melting line flattens (Fig. 1, $0.7 < \phi_1 < 0.9$) by which small variations in temperature result in large compositional changes of the polymer mixture in equilibrium with ice. Consequently, increasing the temperature requires larger amounts of ice to melt in order to accommodate the changes in composition that are required to follow the equilibrium melting line (in Fig. 2 this occurs in the temperature interval −20 °C to −15 °C). At intermediate compositions the melting line becomes steeper again (Fig. 1, $0.5 < \phi_1 < 0.7$) causing smaller changes in composition to be realized. Therefore, a smaller amount of ice needs to melt, seen as a smaller slope in the dilatometric trace. Once this composition interval is passed, the melting line flattens again (Fig. 1, $\phi_1 < 0.4$) generating large compositional changes with increasing temperature, and thus, concomitantly, large volume changes that are reflected in the dilatometric trace (from −10 °C to 0 °C).

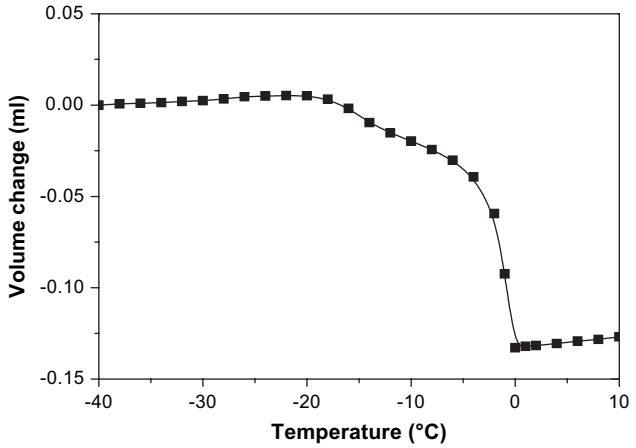

Fig. 2. Dilatometric trace showing the volume change with temperature obtained upon heating (■) after full crystallization of water at −40 °C of a PVME/water sample with $w_{PVME} = 0.2$. Data taken from literature [3].

In DSC those mixtures exhibiting crystallization of water upon cooling are characterized by a double melting endotherm upon heating, consisting of two, more or less separated peaks (examples are given in Figs. 7 and 8, which will be thoroughly discussed in the next paragraph). The shape of the melting endotherm can be related to the derivative with temperature of the melting line. However, the quantitative interpretation along these lines is not straightforward as the DSC experiment is a non-isothermal one, in which consequently the equilibrium situation is not attained.

To fully quantify both the DSC and dilatometric experiments the temperature dependence of the volume and the enthalpy of fusion of ice, as well as the volume and enthalpy of solid and liquid water and the PVME/water solutions that are produced during the ice-melting/water-dissolution process must be known. Since, these data are not that readily available we will present an approximate evaluation of the (MT)DSC melting endotherm, but first we will establish an alternative method employing Fourier transform infrared spectroscopy for determining the equilibrium melting line within the entire concentration interval.

4.2.2. Equilibrium solid–liquid behavior by FTIR

In order to directly determine the composition of the PVME/water mixture coexisting with ice at the investigated temperature the concentration dependence of the C–H symmetrical stretching absorption band of the O–CH_3 group is used.

4.2.2.1. Concentration dependence of the C–H symmetrical stretching absorption band of O–CH_3. FTIR spectra are taken for samples with $0 < w_{PVME} \leq 1$ in the homogeneous liquid state. For each mixture composition the position of the C–H symmetrical stretching absorption band of the O–CH_3 moiety is determined and consequently plotted as a function of concentration (Fig. 3). Note that the C–H symmetrical stretching mode shows a small temperature dependence, shifting with decreasing temperature to longer wavenumber with ca. 0.03 $cm^{-1}\,°C^{-1}$. Therefore, the influence of temperature is minimized by taking each spectrum at ca. 0 °C (in the homogeneous liquid state). The results from Fig. 3 are in good

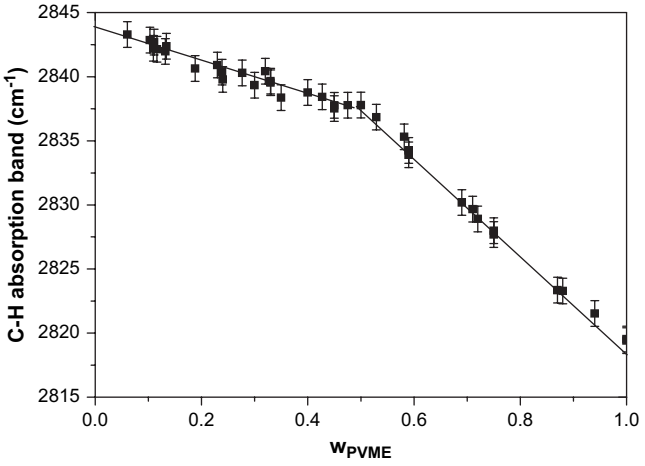

Fig. 3. Concentration dependence of the C–H symmetrical stretching absorption band of the O–CH_3 moiety in homogeneous PVME/water mixtures by FTIR.

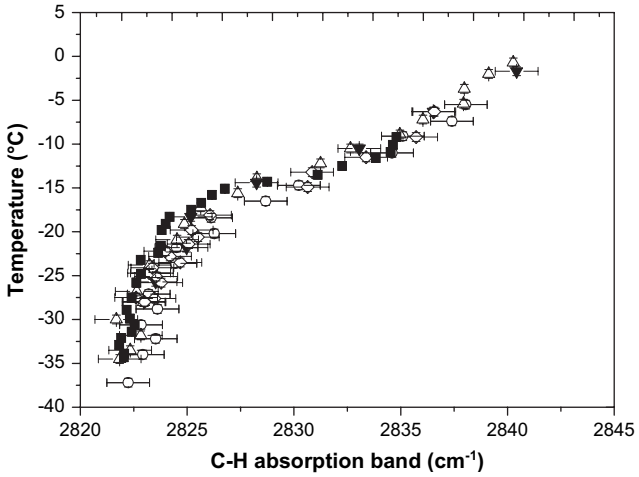

Fig. 4. Wavenumber of the maximum of the C–H symmetrical stretching absorption band of O–CH_3 as a function of temperature obtained from PVME/water mixtures with different overall initial composition: $w_{PVME} = 0.45$ (◇), 0.35 (○), 0.27 (■), 0.23 (△) and 0.15 (▼). Error bars indicate the estimated uncertainties in the FTIR wavenumber readings.

agreement with those reported previously by Maeda [15]. The frequency of the C–H symmetrical stretching shifts linearly to lower wavenumber with increasing polymer concentration, whereas at $w_{PVME} \approx 0.5$ a more pronounced linear concentration dependency emerges.

4.2.2.2. Melting line of water in aqueous PVME solutions. Experiments were carried out using five different samples, for which the crystallization of water occurs directly upon cooling. These mixtures are cooled at ca. 5 °C min^{-1} to −40 °C and kept at that temperature to allow for maximal crystallization of water from the solution. The crystallization of water, which typically finishes within 1 h, is monitored by FTIR (in the 3000 cm^{-1} wavenumber region). Afterwards the sample is stepwise heated, by which at each temperature a certain amount of ice melts. The produced liquid water consequently changes the concentration of the surrounding polymer solution. This finally results in ice coexisting with a PVME/water solution having a concentration according to the solid–liquid equilibrium at that temperature. After the equilibration period, monitored by FTIR, a spectrum is taken and the position of the C–H symmetrical stretching absorption band of O–CH_3 is determined. These results are plotted versus temperature (Fig. 4), coinciding rather nicely for the different concentrations studied.

Using the concentration dependence of the C–H symmetrical stretching absorption band of O–CH_3 (Fig. 3) the wavenumber dependence in Fig. 4 is transformed in the concentration of the PVME solution in equilibrium with ice. In this way the equilibrium solid–liquid line can be determined within the entire concentration range (Fig. 5).

These data allow constructing the average equilibrium melting line, which is presented in Fig. 6, together with the glass transition temperatures of concentrated homogeneous PVME/water mixtures obtained from (MT)DSC experiments (see later). The full experimental melting line of water in the presence of PVME shows a step at intermediate compositions in agreement with theoretical predictions. The location of this step (at ca. −10 °C) is in agreement with the calorimetric and dilatometric measurements from literature [3], which were discussed in the introductory part.

The FTIR experiments enable to determine in situ the composition of the polymer/water mixture in coexistence with ice at any selected temperature of the solid–liquid equilibrium line.

4.2.3. Non-isothermal MTDSC results (heating/cooling) for PVME/H_2O

When cooling a homogeneous PVME/H_2O solution, one expects the solvent to crystallize, as illustrated for a $w_{PVME} = 0.3$ mixture (Fig. 7). Using the total heat flow signal, it can be noticed that for this composition a supercooling of ca. 25 °C is needed to induce crystallization of H_2O (◇, onset crystallization exotherm), when cooling at 1 °C min^{-1}.

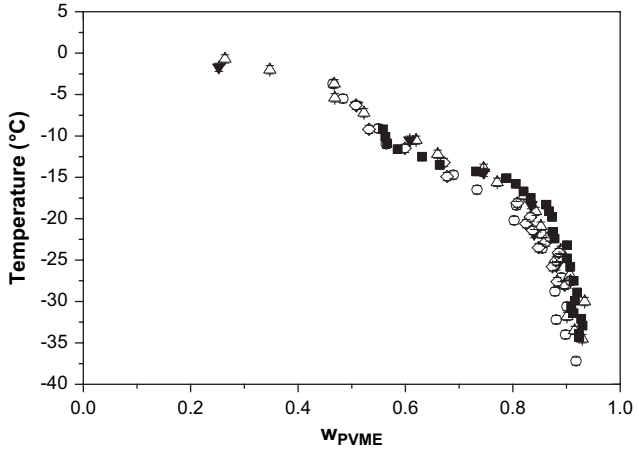

Fig. 5. Solid–liquid equilibrium lines in PVME/water derived from the FTIR data in Fig. 4, for different initial sample compositions: $w_{PVME} = 0.45$ (◇), 0.35 (○), 0.27 (■), 0.23 (△) and 0.15 (▼). The temperature dependence of the band wavenumber was taken into account as explained in the text.

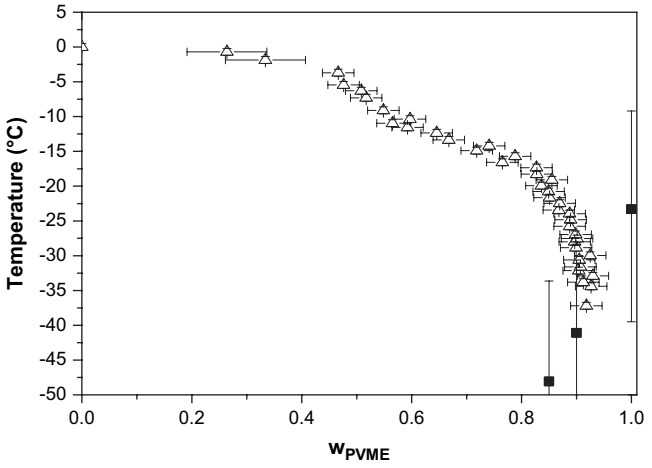

Fig. 6. The average equilibrium solid–liquid coexistence line of water in PVME/water mixtures (△) determined as the average from the individual melting lines obtained from the FTIR experiments at different initial PVME/water compositions (depicted in Fig. 5); and the glass transition temperature of homogeneous PVME/water mixtures as a function of composition (■, width: I). The error bars of the melting line data are also indicated. The temperature dependence of the band wavenumber was taken into account.

The observed crystallization process causes phase separation between ice-crystals and a PVME-rich solution. If the crystallization would occur under isothermal conditions it should either come to an end when the concentrated solution reaches a composition given by the solid–liquid equilibrium (at that temperature) or when the concentrated solution reaches a composition that vitrifies before the solid–liquid equilibrium composition is reached. However, when applying non-isothermal crystallization conditions, cooling to a sufficiently low temperature, as is done in the current MTDSC experiments, will inevitably induce vitrification of the remaining concentrated polymer solution. As a result the devitrification of that glassy PVME-rich phase is observed in the subsequent heating (Fig. 7, inset, ×, indicated by the arrow), followed by the gradual melting of ice (Fig. 7, ●, endset melting endotherm).

Such observation is valid for mixtures having compositions with $w_{PVME} < 0.55$ whereas solutions with w_{PVME} between 0.55 and 0.70 display cold crystallization upon heating (Fig. 8). More concentrated solutions show no crystallization (and thus melting), in agreement with literature [7]. Similar observations hold for aqueous solutions of either poly(*N*-vinyl caprolactam) [6,16] or poly(*N*-isopropyl acrylamide) [4,5], in which the missing crystallization is linked to the interference of vitrification upon cooling, according to the T_g-composition curve. For that reason, the T_g of the homogeneous PVME/H_2O solutions is measured. As expected, T_g lowers with increasing water content (Fig. 8, ■), due to the plasticizing effect of H_2O on PVME.

The experimental transition data obtained from the MTDSC experiments can now be collected to construct part of the state diagram at low temperatures (Fig. 9), including

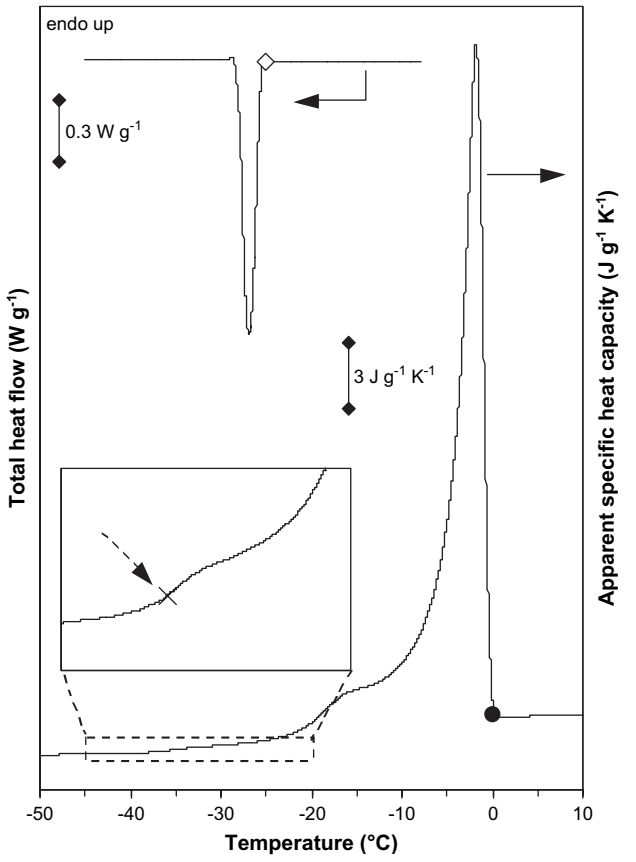

Fig. 7. Non-isothermal cooling (total heat flow) and heating (c_p^{app}) of a PVME/H_2O mixture with $w_{PVME} = 0.30$. Crystallization temperature (◇) upon cooling determined from the total heat flow; T_g PVME-rich phase (see inset: ×, indicated by the arrow) and endset melting endotherm (●) upon heating determined from c_p^{app}.

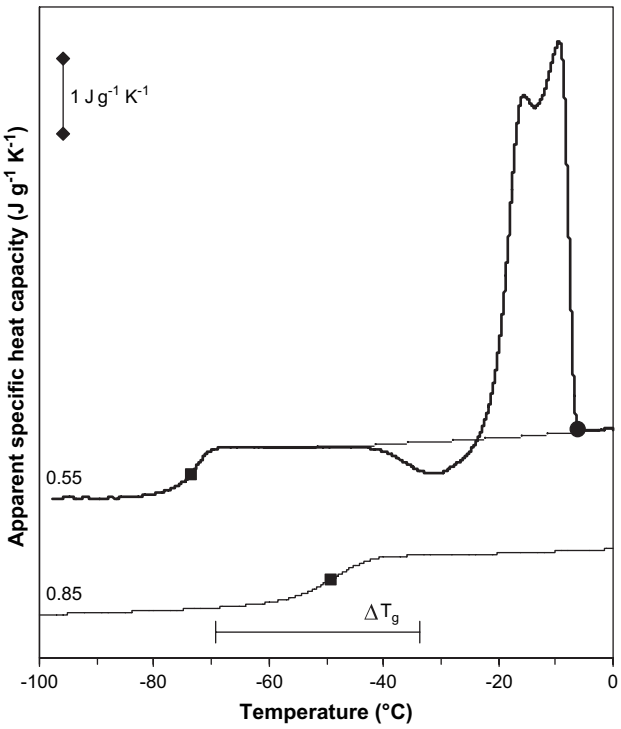

Fig. 8. c_p^{app} during non-isothermal cooling (thin) and heating (thick) of different PVME/H_2O compositions with $w_{PVME} = 0.55$ and 0.85: homogeneous T_g (■) upon cooling and endset melting endotherm (●) upon heating. Curves are shifted vertically for clarity.

among others the T_g-composition curve. The glass transition temperatures of the concentrated homogeneous PVME/water mixtures are shown together with the width of the glass transition region ΔT_g (Fig. 9, ■, width: I). This is of importance, since the possible interference of partial vitrification during crystallization depends on the upper limit of the glass transition rather than on its average value [5,17]. Moreover, the glass transition temperature of the PVME/water mixture that remains after the crystallization of water in the less concentrated mixtures ($w_{PVME} < 0.55$) is nearly constant (Fig. 7, ×) corresponding to the T_g of a homogeneous solution with $w_{PVME} \approx 0.93$ (at ca. −38 °C). This indicates that nearly all solvent was able to crystallize upon cooling.

The onset temperature of the crystallization exotherm is also indicated (Fig. 9, ◇), showing a decrease with increasing polymer concentration, as could be expected. Finally, the melting curve of water in the presence of PVME determined directly by MTDSC (Figs. 9 and 10, ●) does not show a distinctive step in temperature with composition as was theoretically predicted. However, based on the FTIR data the step in the melting line is expected to appear in the composition range where no direct crystallization of water occurs using (MT)DSC.

Alternatively, indications for the predicted peculiar shape of the melting line of the solvent can still be found in the (MT)DSC trace of the melting endotherm (Figs. 7 and 8) as this consists of two more or less separated peaks or a main peak preceded by a shoulder, depending on the polymer concentration. In the case of poly(ethylene oxide) (PEO)/water,

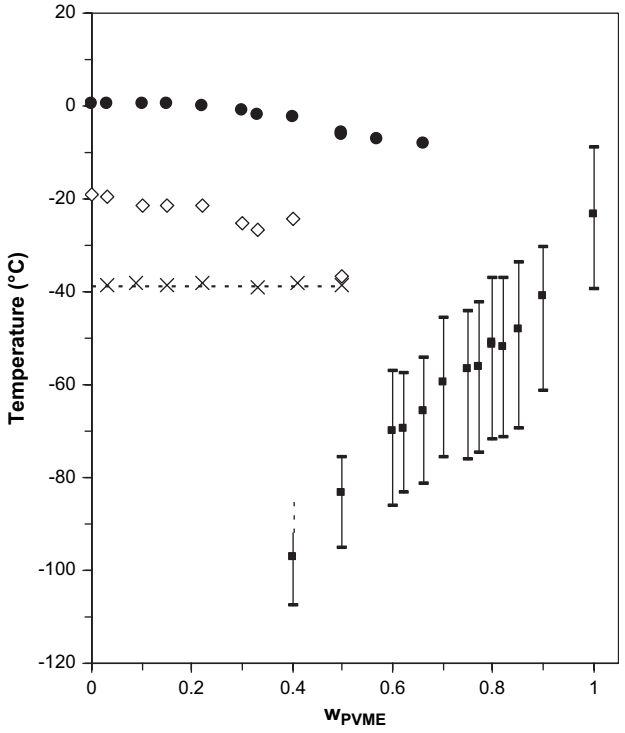

Fig. 9. Part of the state diagram at low temperature (i.e., sub-zero) of PVME/H_2O mixture determined with MTDSC: crystallization curve (◇) upon cooling; T_g PVME-rich phase (×), melting curve (●) and T_g-composition curve (■, width: I) upon heating.

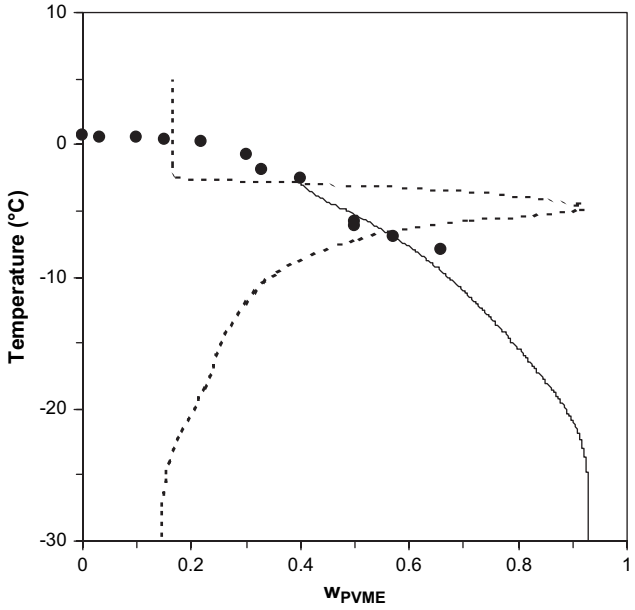

Fig. 10. Change in composition with temperature (continuous line) for PVME/H_2O mixture obtained by partial integration of the melting endotherm (dashed line) after cooling a mixture with $w_{PVME} = 0.40$ to −100 °C, using heat capacity data of pure water and ice. Experimentally determined melting temperatures, obtained from c_p^{app} upon heating for samples of different compositions (●).

for instance, such a double melting endotherm is caused by the presence of a eutectic composition [18,19]. In this case, on the other hand, such peculiar phenomenon cannot be related to eutectic behavior as atactic PVME is unable to crystallize. The most frequently adapted interpretation of the double melting peak in PVME/water mixtures refers to the existence of the bound and free water that melt at different temperatures [20]. However, one must keep in mind that the shape of the melting endotherm is a direct consequence of the concentration–temperature dependence of the melting line of ice, being determined by the thermodynamic solid–liquid equilibrium conditions. Therefore we tried to (partly) reconstruct the change in melting temperature from the shape of one double melting peak observed for one specific composition. Indeed, assuming that the liquid H_2O formed during the melting process quickly remixes with the liquid PVME-rich phase to make the composition of the PVME/water mixture in accordance with the thermodynamic solid–liquid equilibrium, the amount of heat needed up to that temperature (i.e., the partial integrated heat flow) will determine the amount of liquid H_2O formed and as such the new composition of the liquid phase in equilibrium with the remaining ice. In this respect, accurate values of the heat capacity of water and ice are needed in the temperature range of interest [21].

The resulting compositional change with temperature is shown in Fig. 10 for a PVME/H_2O solution with $w_{PVME} = 0.4$. Since after cooling to −100 °C a vitrified mixture with $w_{PVME} \approx 0.93$ is formed, independent of the initial polymer concentration (see Fig. 9, ×), the calculated compositional change at low temperature starts from this composition. The agreement between the melting curve (Fig. 10, continuous

line) calculated from the shape of one particular melting endotherm (Fig. 10, dashed line) and the melting curve determined directly from the endset temperature of the melting endotherm using samples of different compositions (Fig. 10, ●) is rather good, although quantitative agreement is not reached. Hence, the assumptions needed to obtain (part of) the melting line from one non-isothermal (MT)DSC result seem reasonable and appear to hold to a good approximation.

5. Conclusions

The Wertheim lattice thermodynamic perturbation theory was used to predict the liquid–liquid and solid–liquid coexistence data for a model polymer solution. The theory predicts bimodal LCST phase behavior in agreement with experimental results. In addition, the solid–liquid equilibrium of the solvent was calculated and an unusual step with composition is predicted.

In this work an alternative method was developed employing Fourier transform infrared spectroscopy to determine the composition of the PVME/water mixture coexisting with ice, using the concentration dependence of the FTIR C–H symmetrical stretching absorption band of the O–CH_3 moiety at the temperature of interest. This method elucidated that the equilibrium melting line of water in aqueous PVME solutions shows an unusual step with composition, in agreement with the theoretical predictions. Moreover, the shape of the (MT)DSC melting endotherm was correlated to the evolution of the peculiar melting line by partial integration of the melting peak observed. The agreement with the equilibrium melting line determined by FTIR is quite good.

The sudden change in crystallization/melting properties at high PVME concentration is not related to the formation of molecular complexes. It is a direct consequence of the vicinity of the glass transition region, causing a dramatic slowing down in nucleation rate in these highly concentrated polymer mixtures. Hence, due to the peculiar stepwise drop of the melting line at intermediate compositions the actual supercooling becomes smaller than could be anticipated for a conventional course of the melting curve. As a result the homogeneous solution vitrifies and nucleation of the crystalline phase does not occur, unless by adding nuclei, which trigger the nucleation process. So, both the predicted and experimentally confirmed concentration dependences of the melting curve of ice provide a new explanation for the inhibited crystallization at high polymer concentrations. These observations allow to rationalize that the double melting endotherm observed in (MT)DSC is not related to the melting at different temperatures of bound and free water, it simply reflects the peculiar shape of the melting line.

Acknowledgment

Els Loozen thanks the Department of Chemistry of the Katholieke Universiteit Leuven for a PhD-grant. Kurt Van Durme thanks the Institute for the Promotion of Innovation through Science and Technology in Flanders (IWT) for a PhD-grant. The work was supported by the bilateral (international) scientific and technological cooperation of the Ministry of the Flemish Community and the Ministry of Science and Technology of the People Republic of China (BIL01/06). The authors thank the Funds for Scientific Research Flanders (FWO) for financial support.

References

[1] Schäfer-Soenen H, Moerkerke R, Berghmans H, Koningsveld R, Dusek K, Solc K. Macromolecules 1997;30:410–6.
[2] Swier S, Van Durme K, Van Mele B. J Polym Sci Part B Polym Phys 2003;41:1824–36.
[3] Zhang J, Bergé B, Meeussen F, Nies E, Berghmans H, Shen D. Macromolecules 2003;36:9145–53.
[4] Afroze F, Nies E, Berghmans H. J Mol Struct 2000;554:55–68.
[5] Van Durme K, Van Assche G, Van Mele B. Macromolecules 2004;37:9596–605.
[6] Meeussen F, Nies E, Verbrugghe S, Goethals E, Du Prez FE, Berghmans H. Polymer 2000;41:8597–602.
[7] Meeussen F, Bauwens Y, Moerkerke R, Nies E, Berghmans H. Polymer 2000;41:3737–43.
[8] Spěváček J, Hanyková L, Ilavský M. Macromol Symp 2001;166:231–6.
[9] Wertheim MS. J Stat Phys 1984;35:19–34.
[10] Wertheim MS. J Stat Phys 1984;35:35–47.
[11] Nies E. J Chem Phys B, submitted for publication.
[12] Nies E, Li T, Berghmans H, Heenan RK, King SM. J Phys Chem B 2006;110:5321–9.
[13] Nies E, Ramzi A, Berghmans H, Li T, Heenan RK, King SM. Macromolecules 2005;38:915–24.
[14] Chapman WG, Jackson G, Gubbins KE. Mol Phys 1988;65:1057–79.
[15] Maeda H. J Polym Sci Part B Polym Phys 1994;32:91–7.
[16] Kirsh YE, Yanul NA, Kalninsh KK. Eur Polym J 1999;35:305–16.
[17] Van Durme K, Verbrugghe S, Du Prez FE, Van Mele B. Macromolecules 2004;37:1054–61.
[18] Hey MJ, Ilett SM. J Chem Soc Faraday Trans 1991;87:3671–5.
[19] Graham NB, Zulfiqar M, Nwachuku NE, Rashid A. Polymer 1989;30:528–33.
[20] Zhang J, Teng H, Zhou X, Shen D. Polym Bull 2002;48:277–82.
[21] Handbook of chemistry and physics. CRC Press; 1990. p. D-173.